Journal of Molecular Liquids 392 (2023) 123420

Contents lists available at ScienceDirect

Journal of Molecular Liquids

journal homepage: www.elsevier.com/locate/molliq

On the nature of the thermoresponsiveness of poly(2-isopropyl-2-oxazoline) in aqueous solution

Sara Del Galdo [a,*], Carlo Andrea De Filippo [a], Luca Stefanuto [a], Simona Sennato [b], Tecla Gasperi [a,*], Ester Chiessi [c], Barbara Capone [a,*]

[a] Science Department, University of Roma Tre, Rome, Italy
[b] Institute for Complex Systems, National Research Council (CNR-ISC), Sapienza University of Rome, Rome, Italy
[c] Department of Chemical Science and Technologies, University of Rome Tor Vergata, Rome, Italy

ABSTRACT

Poly(2-oxazoline)s (POAs) are a class of biocompatible polymers, that is gaining a prominent role in biomedical field due to its thermoresponsiveness at temperatures compatible with physiologically relevant ones. This work represents the first extensive molecular dynamics simulation study of poly(2-isopropyl-2-oxazoline) (PiPOx) - that is amongst the simplest thermoresponsive POAs - both at infinite dilution as well as finite concentration, aimed at unveiling the thermoresponsive nature of this macromolecular class. Benchmarking simulations against experimental data obtained from specifically synthesized PiPOx's with controlled degree of polymerisation, we can explore the nature of thermoresponsive behaviour. This appears to be dominated by intermolecular interactions that lead to the experimentally observed liquid-liquid phase separation (LLPS). By means of a combined atomistic and coarse-grained approach, we could characterise the polymer rich phase formed upon LLPS, finding average properties of the solution, such as the average distance between polymer chains, that are reminiscent of the experimental lattice pitch measured on crystalline phases. At last, we can hint at the presence of a Liquid Crystalline phase in the polymer rich region at high temperatures.

1. Introduction

Poly(2-isopropyl-2-oxazoline) (PiPOx) is a polymeric amide belonging to the class of poly(2-oxazoline)s (POAs) (see Fig. S1 in the SI for the chemical structure). The hydrophilic tertiary amide of the polymeric backbone is substituted with an isopropylic group which endows the polymer with a lower critical solution temperature (LCST) behaviour in water. This property has made PiPOx, as well as other POAs with the same feature, an optimal candidate for developing smart materials whose solubility is triggered by temperature. In fact, POAs are largely employed for medical and biological applications (such as drug delivery systems or bio-inspired sensors) as they are bio-compatible and have a transition temperature close to that of the human body [1–3]. To broaden the range of possible applications, multi-block copolymers consisting of differently substituted 2-oxazoline monomers, are designed and synthesized to attain a precise tuning of the properties of the resulting macromolecule aimed at achieving predetermined tasks [4–7]. Despite POAs are largely employed for technological applications, even the less complex instances of the family - as PiPOx - are not yet fully characterised. In particular, the molecular origin of thermoresponsiveness of this class of polymers is - to date - not completely unveiled.

Concerning PiPOx, the phase diagram for a range of polymer concentrations was reported for the first time in 2010 [8]; it was shown that PiPOx follows a type I phase behaviour, i.e. the transition temperature (the cloud point temperature, T_{cp}) is affected by the molecular mass. 1 H NMR, Raman, and FT-IR spectroscopy measurements detected that, following de-mixing, the polymer chains dehydrate and undergo relevant conformational transitions. In these conditions, liquid-liquid phase separation (LLPS) occurs [9–11]. Moreover, upon continued heating above the cloud point temperature, the macromolecules crystallise with the formation of a macroscopic precipitate composed of nanofibers [1,9,12–14]. In particular, below the T_{cp} the conformations adopted by the polymer chains are almost disordered and well hydrated (with the macromolecules being dispersed in the solution). Above the cloud point, the polymer adopts an ordered and dehydrated conformation [9–11]. The regular conformation of the polymeric chains reached at high temperature, eventually, drives the formation and precipitation of the crystals [1,9,11]. While crystallisation is an irreversible process, the thermally induced de-mixing is fully reversible [1]. This implies that the stretched conformations achieved at temperatures higher than the T_{cp} are fully reversible prior to the formation of crystals. There is common agreement in literature that the dihedral angles of the chain back-

* Corresponding authors.
E-mail addresses: sara.delgaldo@uniroma3.it (S. Del Galdo), tecla.gasperi@uniroma3.it (T. Gasperi), barbara.capone@uniroma3.it (B. Capone).

https://doi.org/10.1016/j.molliq.2023.123420
Received 19 April 2023; Received in revised form 27 September 2023; Accepted 22 October 2023
Available online 29 October 2023

bone are the degrees of freedom most involved in the conformational transition occurring upon temperature increase. In fact, the chains go from a disordered conformation to a stretched and ordered one while getting dehydrated through large movements of the main chain. Instead, such transition does not relevantly affect the conformations of the side chains [9–11]. However, what drives the conformational change with temperature is not yet clear. In the present contribution we perform a large scale atomistic Molecular Dynamics (MD) simulation study of aqueous PiPOx of diverse degrees of polymerisation at different concentrations, below and above the transition temperature. To the best of our knowledge, this is the first extensive atomistic MD study, supported by experimental data, of aqueous solutions of PiPOx [11,15]. Our aim is to achieve atom-level insights into the interplay between the intra- and inter- molecular interactions that ultimately lead to the LLPS, focusing, amongst the latter, on the role played by hydration. Moreover, we develop a coarse-grained methodology to analyse the finite concentration solutions of PiPOx above and below the LCST mapping each macromolecule onto an effective ellipsoid. The analysis of the relative orientation between the coarse grained macromolecules provides an hint on the presence of a liquid crystalline phase in the solutions above the LCST.

To support and strengthen the theoretical study presented in this work, synthesis and experimental characterisation of PiPOx of different degrees of polymerisation (DPs) have been performed. As the synthesis is extremely sensitive to reaction conditions (solvent, reaction time and initiator) this work has required the optimisation of the synthetic procedure so to have a complete control over the polymerisation process.

2. Methods

2.1. Computational procedures

2.1.1. MD simulations

All MD simulations were performed with the Gromacs 2020 software package [16]. Aqueous solutions of chains of PiPOx of different DP were analysed. Namely, we simulated polymers composed of 10, 20 and 30 repeating units (hereafter, PiPOx10, PiPOx20 and PiPOx30, respectively). Each system was simulated at infinite dilution. Moreover, a finite concentration of PiPOx10 in water was studied at the weight fraction of polymer $x_w = 0.1$. Water was simulated using the TIP4P-Ice model [17]. To model the solute we employed the OPLSAA force field [18] and, to increase specificity of the force field [19], the parameters accounting for the rotation of the dihedral angle N-C-C-N were obtained by using the online LigParGen tool [20] with the dimer of PiPOx (two monomeric units) as input. Moreover, the initial OPLSAA parameterisation of the non bonding parameters was refined by computing QM-level atomic charges on a model compound that mimics the single repeating unit in vacuum. We employed the isobutyl amide substituted with two ethyl groups on the nitrogen atom. The CM5 partial charges have been calculated on the conformation corresponding to the minimum of energy of the model amide. Both calculations have been obtained at the B3LYP/6-311G [21] level of theory with the Gaussian software [22]. From the model compound, we evaluated the atomic charges for the PiPOx atoms by defining three types of residues, namely by considering that each residue may either be: the tail, the head of the polymer (the last and the initial unit of the chain, respectively) or an internal one. Hence, for each residue, the atoms of the model compound not involved in that specific residue were stripped and the corresponding atomic charges were reassigned maintaining the electro-neutrality. The starting conformation of each polymeric chain was designed by fixing the orientation of the carbonyl groups, because of the hindered rotation of the C-N amide bond. We oriented all the carbonyl groups towards the same direction. This configuration was chosen over the one characterised by oxygen atoms facing at each other, on the basis of stereochemical considerations on the mechanism of the polymerisation reaction (see SI, Section 1.2). The scaled atomic charges and the polymeric conformations were obtained by using the antechamber tools provided with the freely available AmberTools package [23]. Both the water model and the OPLSAA force field have been selected as they have shown to successfully reproduce the thermoresponsive behaviour of poly(N-isopropylacrylamide) (PNIPAM) [24].

We performed NPT simulations consisting of 300 ns for the infinite dilution conditions, the first 150 ns being considered for the system equilibration (for the PiPOx30 systems, 180 ns were considered for the equilibration). The $x_w = 0.1$ simulations of PiPOx10 consist of 340 ns with the last 160 ns considered as the production run. We took 1 bar as the reference pressure. As for the temperature, in order to reproduce the system behaviour both below and above the transition temperature, we performed two sets of simulations at T= 283 K and T= 323 K for all the analysed systems. Moreover, for the infinite dilution cases we also performed a set of simulations at T= 303 K. Pressure was controlled using a Berendsen barostat [25] with coupling time of 0.5 ps and isothermal compressibility of $4.5\,10^{-5}$ bar^{-1} while temperature was kept constant by velocity-rescaling thermostat [26]. Integration time step of 2 fs was used. The systems were simulated with periodic boundary conditions. The length of bonds involving hydrogen atoms was constrained using the LINCS algorithm [27]. For short range interactions a cut-off radius of 1.1 nm was employed, while for long range interactions the particle mesh Ewald method was used with grid search and cut-off radii of 1.1 nm [28]. The trajectory sampling frequency was of 0.01 frame/ps. For all the analysed systems, two independent MD simulation replicas have been performed. All reported results are the average computed on both the replicas along with the corresponding standard deviation. Details on the starting configurations for all the systems are reported in the SI (Section 1.1). For the finite concentration systems, the second replicas are performed on systems at the same composition as the original ones but with half the total number of atoms. This allows us to both duplicate the available sampling, and also to exclude the presence of artifacts due to the size of the system.

2.1.2. Analyses of the (ellipsoidal) polymeric shape and the hydration features

Following a recently developed coarse-graining approach [29–31], the atomic-detailed polymeric chains in solution are mapped onto ellipsoids, whose shape is an instantaneous representation of the conformation of each polymer in solution. Such a representation has been shown to be a viable tool to describe macromolecular hydration features [29–31]. The details of the re-mapping are described elsewhere [29–32], however, in the following the basic principles are reported. For each time frame of the simulation, the conformation of the solute (i.e. the polymeric chain), is approximated as an ellipsoid whose semi-axes are obtained from the diagonalisation of the 3×3 covariance matrix of the atomic coordinates of the solute. The eigenvectors of the matrix provide the ellipsoidal axes $(\hat{a}, \hat{b}, \hat{c})$, whose lengths are obtained as a function of the corresponding eigenvalues. Around the ellipsoidal solute, layered coaxial ellipsoids are built by iteratively increasing the value of the semi axes. The number of water molecules, and hence the water density, is then computed within each ellipsoidal layer. Averaging the water density per layer over the MD trajectory provides a characterisation of the hydration profile as a function of the distance from the solute surface. To assess the role played by the presence of the polymer on the average water density - both at infinite or finite dilution - for each MD step, the average ellipsoid (and its layered counterparts) is defined around every macromolecule. The average number of water molecules contained within the ellipsoid is then computed, and normalised to the number of bulk water molecules that would be contained within the same ellipsoidal volume reduced by the volume occupied by the polymer chain within the ellipsoid. Computationally, this is achieved by superimposing the polymeric coordinates to a box of pure water (randomly sampled from a reference simulation of pure TIP4P-Ice) and removing all the water molecules whose atoms are at a distance from the polymer ones smaller or equal to the sum of the two

van der Waals radii [33,34]. By iterating such a calculation on all snapshots, a "fictitious" hydration profile is computed for every system and compared with the one obtained from the corresponding trajectories of all analysed polymer simulations (finite or infinite dilution). The ratio between the two estimated hydration profiles, provides the change in water density with respect to the bulk due to the presence of the polymers (ρ/ρ_{fict} profiles). Finally, the dimension of the hydration shell can be extrapolated from the density profiles as the distance from the polymer surface at which $\rho/\rho_{\text{fict}} = 1$. As a consequence, an estimate of the volume of the hydration shell can be obtained by adding such a value to the semi-axes of the polymer ellipsoid. The number of water molecules included within this volume hence can be employed to evaluate the water density increase due to hydration [29–32].

2.1.3. Analyses of the chains arrangement and alignment

The spatial arrangement of the polymeric chains - in the case of finite concentration - can be determined by computing the three dimensional pair distribution function of the centres of mass of the macromolecules.

The standard radial pair distribution function $g(r)$ is defined as:

$$g(r) = \frac{1}{4\pi\rho r^2 N}\left\langle \sum_{i}^{N}\sum_{j\neq i}\delta(r - r_{ij})\right\rangle \tag{1}$$

where $\rho = N/V$ is the density of the system, with N and V the number of particles and the volume of the simulation box, respectively, r_{ij} is the modulus of the distance between the centre of mass of chains i and j, $\delta(r - r_{ij})$ is the Dirac function which gives 1 if $r = r_{ij}$, and the angle brackets represent the ensemble average.

Additional information on the average properties of solutions at finite concentration, can be found by looking at the average relative orientation of the macromolecules. The latter can either distribute randomly with respect to the others, or - eventually - local alignment can be found.

To assess whether the molecules align, we adopt the coarse graining strategy described in the previous section, by mapping each polymer onto its corresponding ellipsoid.

Every ellipsoid is described by means of its 3 axes a, b and c; for each i-particle we introduce $\mathbf{u}_i^J = (u_{i,x}^J, u_{i,y}^J, u_{i,z}^J)$ as the unit vector describing the orientation of each axis $J \in [a, b, c]$ of the ellipsoid in the laboratory frame. We introduce the ordering matrix tensor $Q_{\alpha,\beta}^J$:

$$Q_{\alpha,\beta}^J = \frac{1}{2N}\sum_{i}^{N}\left(3\langle u_{i,\alpha}^J u_{i,\beta}^J\rangle - \delta_{\alpha,\beta}\right) \tag{2}$$

For each J-axis of the particles, the order parameter S^J is defined as the largest amongst the three eigenvalues of the ordering matrix $Q_{\alpha,\beta}^J$. The corresponding eigenvectors $\mathbf{n}^J$ indicate the nematic directors. The bigger the S^J the greater the alignment of the system along the $\mathbf{n}^J$ direction. If every S^J is smaller than a threshold r_c the system is considered to be isotropic. As soon as one of the three $S^J \geq r_c$, nematic order arises.

If more than one $S^J > r_c$, the nematic axis is defined by the $\mathbf{n}^J$ coupled to the greatest amongst all S^J. An interesting glimpse over the emergence of a preferential orientation within the system, can be obtained analysing the 3D pair distribution function defined as

$$g^{3D}(\mathbf{r}) = \frac{1}{\rho N}\left\langle \sum_{i=1}^{N}\sum_{j\neq i}\delta\left(\mathbf{r} - (\mathbf{r}_i - \mathbf{r}_j)\right)\right\rangle \tag{3}$$

along planes that are parallel and perpendicular to the nematic one. For every frame, the diagonalisation of $Q_{\alpha,\beta}^J$ defines the three orthogonal axes along which the $g^{3D}(\mathbf{r})$ are computed.

To unveil the angular correlation between ellipsoids at a distance r, we introduce the orientational radial pair distribution function $g_2(r)$:

$$g_2(r) = \langle P_2(\cos(\theta_{ik}(r)))\rangle \tag{4}$$

where P_2 is the second order Legendre polynomial $P_2(\cos(\theta_{ik}(r))) = (\cos^2(\theta_{ik}(r)) - 1)/2$, $\cos(\theta_{ik}(r)) = \mathbf{u}_i^J \cdot \mathbf{u}_k^J$, $J \in [a, b, c]$, and $\theta_{ik}(r)$ is the angle between the axes $\mathbf{u}_i^J$ and $\mathbf{u}_k^J$ of the i-th and k-th particles.

2.2. Experimental methodology

Unless otherwise stated, solvents and common reagents were purchased from commercial sources without any further purification (Sigma-Aldrich). Methyl tosylate (98%) was purified by distillation at reduced pressure and stored under Argon atmosphere. Acetonitrile (ACN) (HPLC gradient grade) was distilled over calcium hydride (CaH_2) and stored under Argon atmosphere. The reaction mixtures were analysed with a SHIMADZU GC-2010 with a capillary column of SLBTM-5ms (30 m × 0.25 mm × 0.25 μm) coupled with a Mass Spectrometer SHIMADZU QP 2010S; the mass values are reported as mass/charge ratios (m/z). All spectra were measured with a column temperature program from 50 °C to 250 °C and the injection temperature was set to 250 °C. The weight-average molar mass (M_w) and the number-average molar mass (M_n) of each polymer were measured by means of Gel Permeation Chromatography (GPC) analyses performed using an Agilent 1260 Infinity II instrument equipped with a Diode Array Detector (DAD 1260 Infinity), an Agilent 1260 Infinity online degasser and an Agilent 1260 Infinity automatic liquid sampler. The GPC setup consists of three columns in series: a precolumn (Phenogel 5 μm Linear/Mixed, LC Guard Column 30 × 4.6 mm) followed by two columns Phenogel 5 μm 10 E5 Å (300 × 4.6 mm) and Phenogel 5 μm 10 E3 Å with a separation range of (10-1.000 K) and (1-75 K) respectively. Samples were injected with a concentration of 1.5 mg/mL and measured at 25 °C using DMF 50 mM LiBr as eluent, 0.27 mL/min flow. Polystyrene reference materials (provided by Alfa Aesar) with M_w = 1.3 kDa (M_w/M_n = 1.10), M_w = 65 kDa (M_w/M_n = 1.06), M_w = 290 kDa (M_w/M_n = 1.06), M_w = 650 kDa (M_w/M_n = 1.06) and M_w = 900 kDa (M_w/M_n = 1.10) were employed for calibration curve.

2.2.1. Synthesis of 2-isopropyl-2-oxazoline

2-Isopropyl-2-oxazoline was synthesized by a modified Witte-Seeliger cyclocondensation of isobutyronitrile (1 eq) with 2-aminoethanol (1.2 eq), and zinc acetate hydrate (0.02 eq) as catalyst. The reaction mixture was kept under stirring at 130° °C for 36 h with an Argon flow passing through the reaction vessel [35,36]. The crude product was dissolved in dichloromethane (DCM) and extracted several times with water. The organic phase was dried over anhydrous magnesium sulphate and dried in vacuo. The product was purified by vacuum distillation over NaOH (50 mbar, 55 °C) followed by overnight stirring over CaH_2 and subsequently vacuum distillation under Argon atmosphere. The pure product was obtained as a colourless liquid in 70% yield. GC-MS: Retention time: 7.7 min, m/z = 113 (M^+) ^{1}H NMR (600 MHz, $CDCl_3$): δ = 1.08 (d, J = 6.5 Hz, 6H), 2.47 (dq, J = 8.5 Hz), 3.71 (t, J = 9.4 Hz, 2H), 4.12 (t, J = 9.5 Hz, 2H) ppm. ^{13}C NMR (150 MHz, $CDCl_3$): δ = 167.1, 67.4, 54.1, 31.1, 19.3 ppm.

2.2.2. Synthesis of poly (2-isopropyl-2-oxazoline)

The Cationic Ring-Opening Polymerisation (CROP) of 2-oxazolines follows a typical chain-growth polymerisation mechanism via initiation, propagation and termination [37]. A two-neck round bottom flask equipped with an efficient reflux condenser and a magnetic stirring bar was charged with 2-isopropyl-2-oxazoline (20 mmol) and anhydrous ACN (10 mL). The system was kept under Argon atmosphere. The reaction mixture was placed in an oil bath at 90 °C and the polymerisation was started by adding the initiator (methyl tosylate) in a suitable amount with respect to the desired polymer chain length. After 24 h, the reaction was quenched by adding a solution of NaOH 1M (excess to the initiator) and the resulting mixture was stirred for 2 h. The solvent was evaporated under vacuum and the residue was added to a solution of petroleum ether: diethyl ether (1:1). The polymer was recovered as a white precipitate, the supernatant was removed, and the product was

washed twice with the petroleum ether: diethyl ether solution and dried in vacuo. Both the weight-average molar mass and the number-average molar mass of each polymer were measured by means of GPC analyses. Specifically, we observed M_w = 3.39 kDa, 5.54 kDa and 9.83 kDa, respectively for the shortest, medium and longest polymer chains, and M_n = 3.08 kDa, 5.04 kDa and 8.94 kDa; while the polydispersity index is M_w/M_n = 1.11, 1.10, 1.10.

2.2.3. Dynamic light scattering

Dynamic light scattering (DLS) measurements were carried out by a Malvern Zetasizer Nano-ZS in backscattering configuration i.e. the scattered light is collected at an angle of 173°. This detection geometry is less sensitive to multiple scattering effects [38] and also helps to reduce the effects of the presence of dust or of large irregular aggregates on the size distribution, since large particles mainly scatter in the forward direction. The measured autocorrelation functions of the scattered light intensity were analysed using the NNLS algorithm [39] to obtain the distributions of the hydrodynamic radius, that was converted to a diffusion coefficient distribution. The average diffusion coefficient was evaluated by the position of the peak maximum and the standard deviation represents the width of the size distribution. Samples were dissolved in Milli-Q water at a concentration of 1 mg mL^{-1} and filtered with regenerated cellulose (RC) filter (0.45 μm). Temperature was fixed at 298 K.

3. Results

3.1. High temperature prompts stretched conformations of PiPOx

Aqueous solutions of PiPOx at infinite dilution, for different DPs, were simulated above and below the T_{cp}. The aim is to unveil, at the single chain level, both hydration and preferential conformations achieved by the polymer in response to a change in temperature. The three solutes selected, namely, PiPOx10, PiPOx20 and PiPOx30 (see Methods), are employed to model the behaviour of aqueous solutions of the PiPOx of molar mass around 1, 2 and 3 kg mol^{-1}. In general, for aqueous PiPOx, the T_{cp} depends both on the polymer molar mass and on the concentration of the solution. Literature reports that PiPOx LCST spans from 307 K for the polymer with M_n of 3.3 kg mol^{-1} at $x_w = 0.3$; to 299 K for M_n of 13 kg mol^{-1} at $x_w = 0.2$ [8]. Experimental data relative to the particular systems analysed in this work (for the combinations of molar mass and concentration studied) are not available, thus we have no preliminary information on the actual T_{cp}. Nevertheless, we expect our T_{cp}s to be consistent with the ones reported in literature ($T_{cp,av} \sim 300K$). This motivates our choice of selecting two temperatures, one - T_L- well below and the other - T_H - well above $T_{cp,av}$ to assess the thermoresponsiveness of the system. Moreover T_L and T_H are chosen to be distant from both the freezing and the boiling point of water. All considerations brought us to define T_L = 283 K and T_H = 323 K to model the thermodynamically stable solution and in de-mixing condition, respectively (see Methods). To compare our results to experimental data, we add an analysis of the infinite dilution cases (single molecule in water) at room temperature condition (i.e. T_R = 303 K). In particular we compare the computational trend of the diffusion coefficient (D) as a function of DP, with the one measured on our samples by means of DLS experiments (see Methods) at ambient temperature. Computationally, we apply the Einstein relation to compute D from the mean square displacement of the centre of mass of the chains, as computed by Gromacs2020 [40]. The comparison between the computed and measured data is reported in Fig. 1. Exact matching of the results cannot be expected; the computational data, reproducing the order of magnitude of D, are in agreement with the experimental ones, thus contributing to the validation of our computational results.

As described in the Introduction, both the polymeric rich phase above the T_{cp}, and the PiPOx crystals are characterised by stretched conformations [9,10]. We thus started our analysis by addressing the differential average conformations of the macromolecule at the different simulated temperature. For all the infinite dilution cases, the radius of gyration R_g is computed, as shown in Fig. 2 where R_g is reported for the three temperatures (i.e. T_H, T_R, T_L) as a function of the molar mass. The effect of temperature on the average size of the macromolecule is evident: while R_g grows as a power law as a function of the molar mass (M) for the systems at $T = T_L$, the high temperature case T_H is characterised by a quasi linear growth. In fact, when the curves are fitted according to the scaling law $R_g \approx aM^{\nu}$ [41], we obtain $\nu_{T=283K} = 0.54 \pm 0.14$, $\nu_{T=303K} = 0.88 \pm 0.02$, $\nu_{T=323K} = 0.86 \pm 0.04$. The quasi-linear dependence of R_g on the molar mass at T_R, similar to the one obtained at high temperature, and in contrast with the power dependence found at T_L, indicates that, in our simulations, T_R is about the transition temperature, as experimentally expected. The fitting of the data does not change if an additional point corresponding to the dimer is included in the curves (see SI, Section 2.1). For completeness, we also included in the SI the curves showing the trend of the end-to-end distance as a function of the polymer mass.

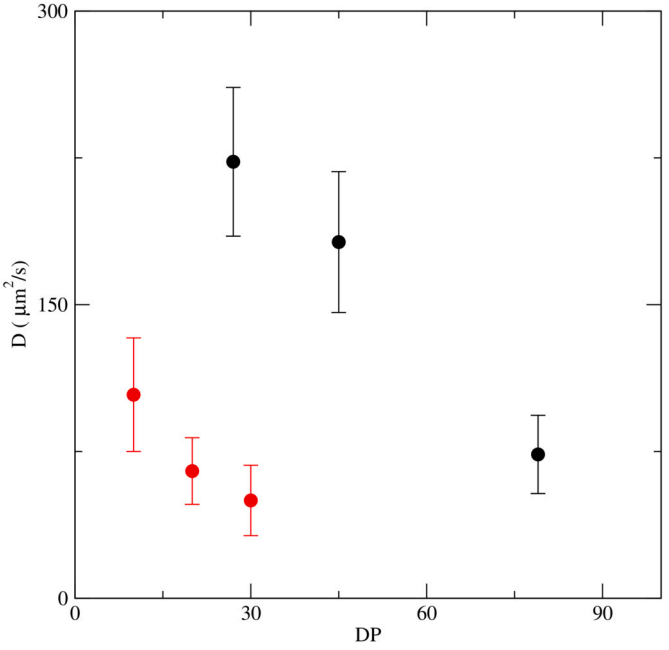

Fig. 1. Diffusion coefficient (D) of PiPOx as a function of the DP for the single molecule aqueous solutions at room temperature. Both computational (red dots) and experimental (black dots) results are reported. For the computational data we set the temperature $T = T_R = 303$ K; the data are averaged over two independent replicas and the corresponding standard deviation is reported. The reported values of the diffusion coefficient correspond to the average values over three repeated measurements. The error reported on the experimental data is obtained from the width of the diameter distribution.

DLS experiments allow to evaluate the hydrodynamic radius of a macromolecule in solution as the radius of an effective sphere that moves as a Brownian particle. In the analysed systems this spherical assumption seems to be too strong to expect a favourable comparison with the computational data of the gyration radius. Moreover, the evaluation of hydrodynamic radius may be flawed due to the presence of a layer of solvent surrounding the polymer coil while it diffuses. For these reasons, it is well known that a direct comparison between a theoretical radius of gyration and an experimental hydrodynamic radius (R_h) is not straightforward. In addition, even if the macromolecule would have an average spherical conformation, the comparison between the gyration radius obtained computationally and the experimental hydrodynamic radius R_h is not straightforward. According to the specific nature of a system and the corresponding hydration features, we can thus expect either $R_g \geq R_h$ or $R_g \leq R_h$. For this reason we selected the diffusion

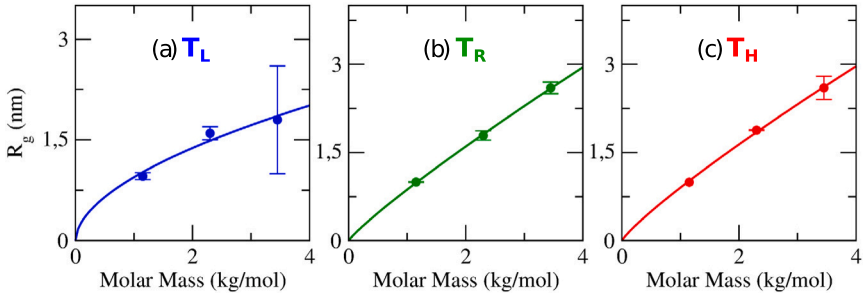

Fig. 2. Radius of gyration (R_g) of PiPOx as a function of the polymer molar mass for the single molecule aqueous solutions below the T_{cp}, at room temperature and above the T_{cp} (i.e., $T = T_L = 283$ K, $T = T_R = 303$ K and $T = T_H = 323$ K, respectively). While the T_L systems grow with a power law as a function of the molar mass, the trend of R_g as a function of the polymer molar mass at high temperature is shown to grow almost linearly with the molar mass: at high temperature conditions every increase in repeating units leaves the chain unfolded (the fitting curves are reported as full lines in each plot).

coefficient, rather than the radius of gyration, as the observable for evaluating the agreement between experiment and simulation (Fig. 1).

The stretching of the polymer is governed by the conformation of the backbone, which depends on the rotations around the CC and the CN bonds. As shown in Fig. 3 (panel (a)), two independent dihedral angles describe such rotations, namely the Φ and Ψ dihedral angles. We defined Φ and Ψ trough the quadruplets of atoms on the backbones N-C-C-N and C(O)-N-C-C, respectively (where C(O) represents the carbon of the amide moiety while C represents the aliphatic carbon atom in the main chain). From the simulations of PiPOx20 at infinite dilution at low and high temperature, we computed the instantaneous values of each Φ and Ψ dihedral angle along the trajectory thus obtaining the two-dimensional histograms reported in Fig. 3 (panel (b) and (c)). For clarity, in the same figure, the corresponding histograms of Φ and Ψ - taken separately - are also reported. Both systems show a pronounced peak in the region $(\Phi, \Psi) \approx (\pm 180, -90)$ which corresponds to polymeric chains in stretched conformations with the isopropyl groups alternatively oriented upward and downward from the backbone plane. By comparing the two panels in Fig. 3, it clearly emerges that small deviations from such behaviour are responsible for the different macroscopic average conformations that characterise the low and high temperature simulations (and that provide the different R_g values reported in Fig. 2). In fact, the few values of Φ in the interval $[50, 90]$ obtained for the low temperature system, correspond to regions along the backbone where the series of trans dihedral conformation is interrupted and the structure partially folds. In Fig. 4 we report snapshots extracted from the two simulations to represent the two different PiPOx20 average conformations at T= 283 K and T= 323 K. The average conformation that we obtain for the high temperature simulation mirrors the structure experimentally obtained from the PiPOx crystals. Not only the stretched conformation of the backbone and the axial alternating disposition of the side chains are reproduced computationally, but also the periodicity in the chain which is experimentally reported to be 6.4 Å [11,14,42]. In fact, when computing the pairwise distance between second nearest neighbour N along the main chain, we obtain a value of 6.5 Å± 0.2 (this value is computed by averaging the time-average distances obtained for each couple; the result is the same for all the dilute solution simulations). Note that the conformational analysis reported above provided analogous results when applied to both PiPOx10 and PiPOx30 infinite dilution simulations (see SI, Section 2.2).

3.2. Thermoresponsiveness in aqueous PiPOx is driven by inter-molecular interactions

The results reported in the previous paragraph show unambiguously that, when temperature is above the cloud point, the polymers preferentially adopt elongated conformations, that are reminiscent of those experimentally found for the PiPOx macromolecules when they assemble a crystalline phase. The immediate consequence is that, differently to other known thermoresponsive polymers, as for example PNIPAM [24], the de-mixing process does not involve an intramolecular collapse. To gain insight on the phase domain within the mixing gap and explore the interplay between the chains, we performed an in depth investigation of a finite concentration of aqueous PiPOx10, at the two temperatures T_H and T_L defined in the previous section.

We report in Fig. 5 two representative snapshots extracted from the finite dilution simulations performed at the two considered temperatures. Fig. 5 clearly shows that for $T<T_{cp}$, even if some extent of aggregation can be observed, the PiPOx chains are well hydrated, and sparse polymeric clusters can be observed; on the contrary, above the cloud point, only one cluster enclosing all the solute molecule is formed. Such a condition is consistent with the LLPS which is known to characterise the PiPOx aqueous solution de-mixing. The Solvent Accessible Surface Area (SASA), computed by considering all the solute chains together [43], confirms that - on average - at high temperature the polymeric chains form a compact cluster. In fact, SASA per chain is 8.3 ± 0.2 and 5.5 ± 0.6 nm^2 for the systems below and above the transition point, respectively: the smallest value clearly reports on the increased average compactness of the polymeric cluster at high temperature. However, the values of SASA corresponding to the infinite dilute simulations of PiPOx10 at T_L and T_H are 16.8 ± 0.3 and 17.2 ± 0.3 nm^2 respectively. We can thus conclude that even for the T_L case some clustering can be appreciated, as the corresponding SASA value is around half of that of the single chain in solution. Qualitatively, the fact that some degree of aggregation is detected even in the T_L case, is to be expected as, in general, experimental solutions of aqueous PiPOx at the mass fraction of about 0.1 do not appear completely transparent, suggesting the presence of supramolecular structures of polymeric particles that act as visible light scattering centres (see SI, Figure S1).

We move forward in the investigation of the properties of finite concentration solutions, by using the introduced coarse grained remapping of polymer chains onto ellipsoids. We use such a simplified description to investigate how the polymers interact with one each other as a function of temperature, and to assess whether the change in flexibility of the single polymer chain that has been demonstrated in the single macromolecule investigation, affect local and global properties of finite concentration solutions.

Even in their elongated structure, polymers remain soft molecular objects, thus the remapping of the atomistic description onto effective ellipsoids retains the conformational fluctuations, as can be seen in panel (a) and (b) of Fig. 6 where the distribution of the values of every axis of each ellipsoid is reported.

The axes reported in panel (a) for the lower temperature show a broader distribution with respect to the ones in panel (b), that are more peaked around their mean value. This confirms the fact that less fluctuations are to be expected at higher temperatures, and more elongated structures are to be expected in this condition.

Within the coarse representation, we compute the spatial arrangement of the chains, by means of the pair radial distribution function

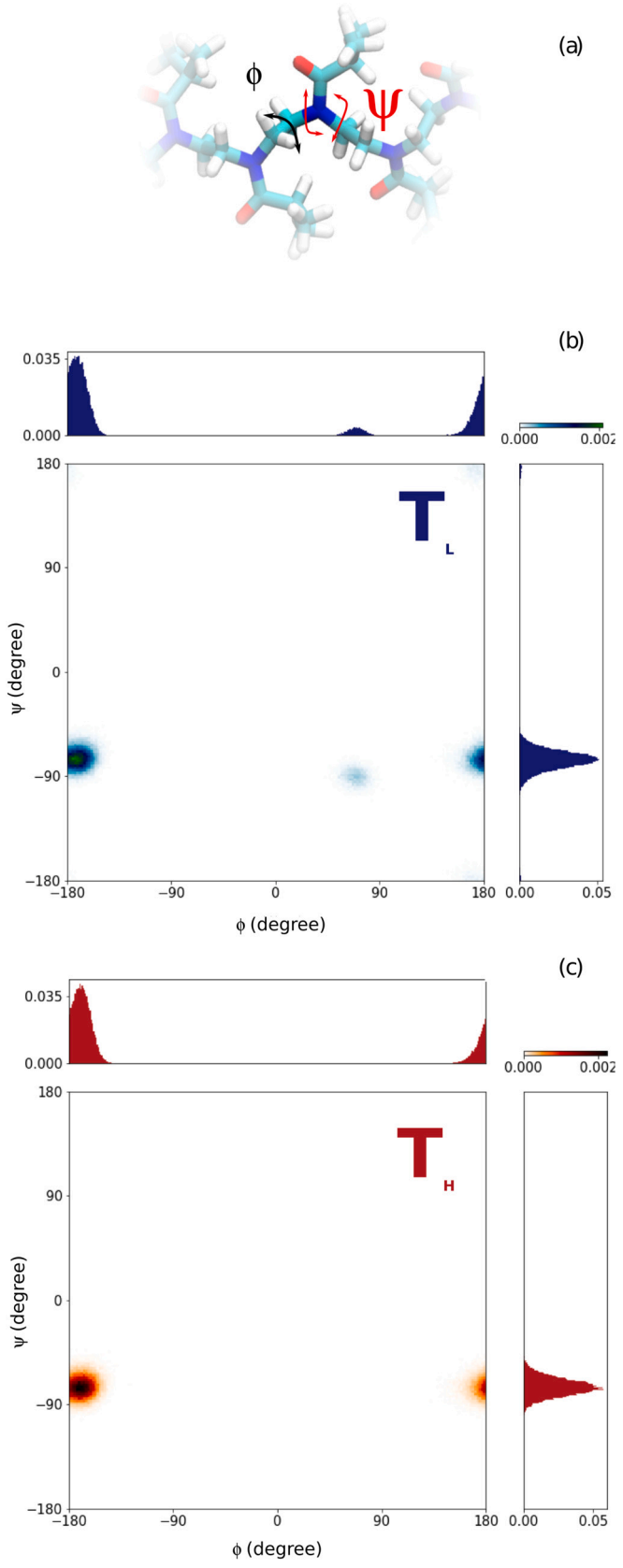

Fig. 3. Panel (a): Non-redundant Φ and Ψ dihedral angles that determine the conformations of the PiPOx main chain. Panel (b): Mono and bi-dimensional histograms of the Φ and Ψ values characterising the conformations of PiPOx20 at infinite dilution at T= 283 K. Panel (c): Mono and bi-dimensional histograms of the Φ and Ψ values characterising the conformations of PiPOx20 at infinite dilution at T= 323 K. Data from both replicas are employed to realise the plots.

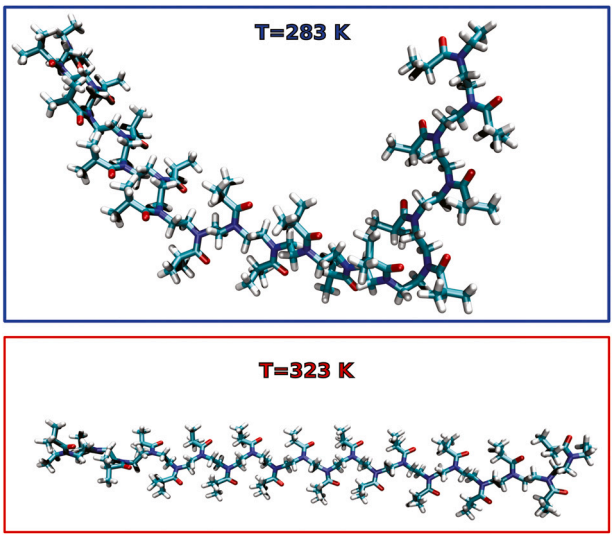

Fig. 4. Representative snapshots extracted from the aqueous PiPOx20 simulations at T= 283 K and T= 323 K. While in the former case the polymer average conformation is slightly folded, the macromolecular chain at high temperature is steadily stretched into all-trans conformations. A periodicity of 6.5 Å is obtained for the high-temperature conformation, in line with the X-ray data measured from the polymer crystals.

$g(r)$, and compare the average distribution of chains at low and high temperature as reported in panel (b) of Fig. 6.

The direct comparison between the high temperature and low temperature shows that in both cases the $g(r)$ are characterised by four peaks. By defining the axes of the ellipsoids as $a > b > c$, the 4 peaks can be rationalised in terms of the distance between couples ij of ellipsoids, and they can be considered to be compatible with situations in which both ellipsoids have their a axes parallel and (i) the particles are stacked along the c axes, (ii) either particles belong to the case (i) and their c axes are greater than the mode of the distribution, or they are stacked and the c_i axis of the i-th ellipsoid is parallel to the b_j axis of the j-th one, (iii) particles are stacked, their c_i and b_j axes are parallel and greater than the mode of the distribution, and (iv) the particles are stacked along the b axes. Nevertheless, even if the peaks of the two radial distribution functions fall in the same region, their height is different, implying that particles have a stronger probability to align at high temperature.

We can move forward in the analysis by computing the orientational pair distribution function $g_2(r)$ between couples of coarse macromolecules for the two temperatures analysed as reported in Fig. 7. The $g_2(r)$ is computed as the average angular orientation between couple of ellipsoidal axes ($g_{2aa}(r), g_{2bb}(r)$ and $g_{2cc}(r)$). It is immediate to appreciate that, while for low temperature (T_L) (panel (a) of Fig. 7) the $g_2(r)$ computed for all couples of axes are compatible with one another and no preferential alignment emerges, at high temperature (T_H), the orientational order is strong. Panel (b) of Fig. 7 in fact, shows that all $g_2(r)$ have a first peak at the same distance, meaning that particles have a strong tendency to completely align (nematic biaxial alignment). Such a peak in the T_H $g_2(r)$ corresponds to the first peak of the $g(r)$ in the T_H pair distribution function reported in panel (b) of Fig. 6. This implies that particles at T_H have a strong tendency to align along all of their axes.

It is interesting to analyse the nematic order parameters at low and high temperatures to investigate whether the order extends further than first neighbours. We report in Fig. 8 the order parameters for low (panel (a)) and high (panel (b)) temperatures, around the three axes of the particles. By comparing the values of the order parameters at low and high temperature, it is immediate that the order parameter of the a axis boosts when temperature is higher than the transition temperature. This

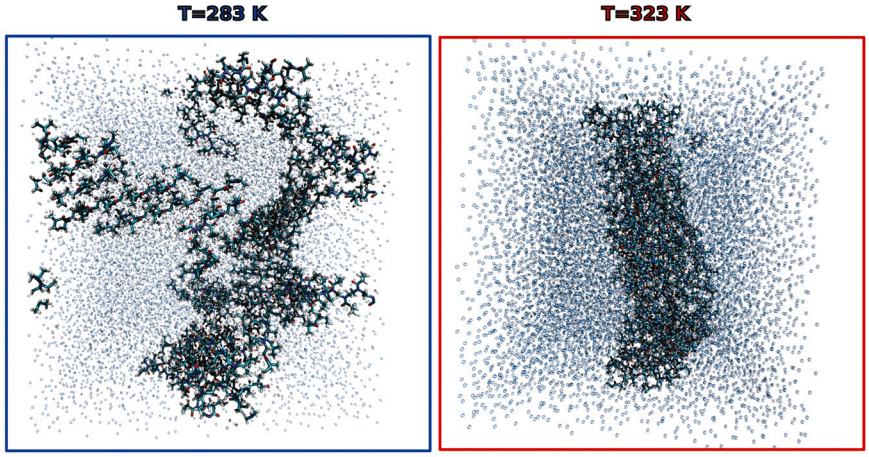

Fig. 5. Representative snapshots extracted from the aqueous PiPOx10 simulations at $x_w = 0.1$, for the T= 283 K and T= 323 K cases. Polymers are highlighted through the licorice representation, while water is represented through lines. While at $T<T_{cp}$ the polymer chains clusterize while remaining well hydrated, liquid liquid phase separation occurs above the T_{cp}.

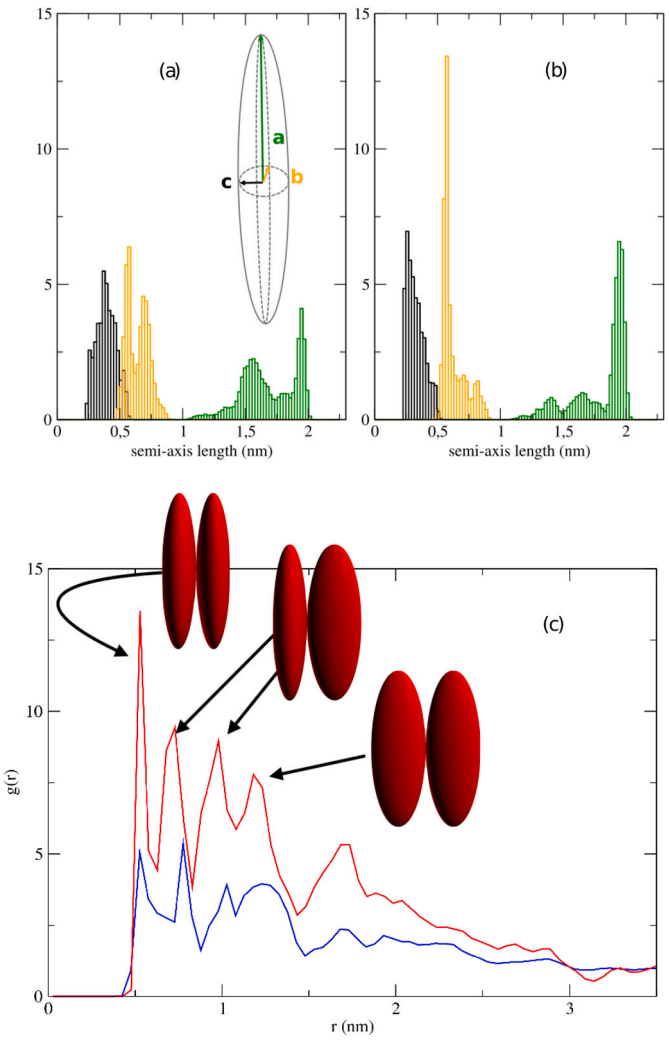

Fig. 6. The distribution of the three axes of the ellipsoids at low temperature T= 283 K (panel (a)) and high temperature T= 323 K (panel (b)); in black c, in orange b and in green a. Panel (c): The radial distribution functions computed between the centres of mass for low (blue) and high (red) temperature. The two $g(r)$ present 4 peaks that correspond to different preferential alignments as sketched.

implies that long range order is present in solution and - in average - all particles tend to align their principal axes.

At last, another method that we use to characterise the changes in the spatial arrangement of particles in solution as a function of temperature, is the analysis of the $g(r)$ on two specific planes (see $g^{3D}(r)$ in Methods). The first plane, that we will call $z = 0$, is the one orthogonal to the nematic axis (as defined in the Method section); the second one is $x = 0$, that is a plane parallel to the nematic axis. The T_L/T_H comparison of this 2D representation of the $g^{3D}(r)$ shows that in the T_L cases (panels (a) and (c) of Fig. 9) there is no preferential spatial order amongst particles. In the T_H case instead, particles are confined in a sub portion of the simulation box (abundance of the white region in panel (b) and (d) of Fig. 9), and the average distances occupied by the particles orthogonal to the nematic axis are the well defined ones obtained by the standard $g(r)$ analysis in Fig. 6 and here highlighted by the red circles in panel (b). By analysing panel (d) it is instead possible to appreciate that particles tend to align along the nematic axis, as indicated by the two darkest regions. The latter demonstrates that it is highly probable to find two nearest neighbours stacked. Moreover, the elongated nature of the non zero probability region in panel (d) indicates that particles tend to assemble, along the nematic axis, in a confined tubular configuration. In the same Fig. 9, we report two representative snapshots of the T_L and T_H systems where the polymer chains are mapped onto the effective ellipsoids according to the coarse grained representation. In the SI, Section 3, we report the results of the same analyses obtained from the $x_w = 0.1$ replica.

Our analysis has not reached concentrations where crystallisation would occur spontaneously. Nevertheless the high temperature order that has been discussed in this section, can be hypothesised as a precursor of long range crystalline order, thus it is interesting to compare our theoretical predictions to experimental results on crystals [14]. Experimentally, the crystals of PiPOx are made of stiff polymer chains regularly aligned along all the three molecular axes. All axes of the crystallised molecules align with a periodicity along the shortest molecular axis (that in our coarse representation is the c axis) of 4.85 Å [14] The agreement between the experimental findings and our coarse prediction is striking, as we find that in our tubular aggregates at high temperature, the average distance between particles along the c axis of the ellipsoids is about 5 Å.

The presence of such structural pattern suggests that locally, above the transition temperature, the chain conformation resembles that adopted in the crystal, and that the aligned structures might act as crystallisation nuclei driving the formation of crystals upon dehydration and continuous heating.

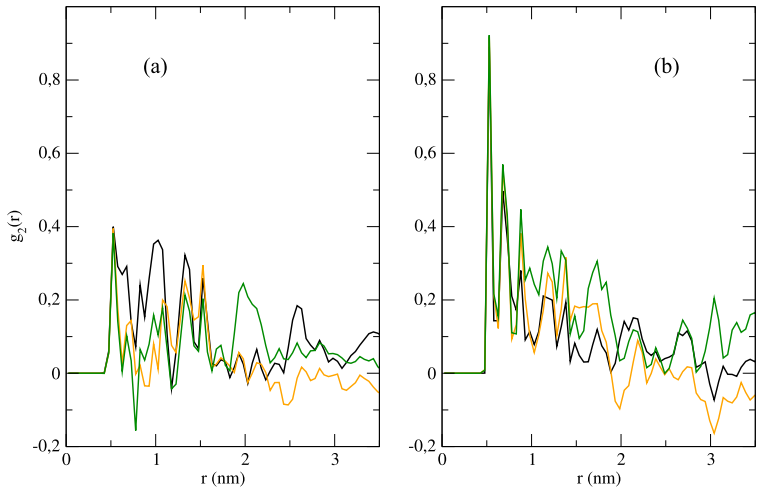

Fig. 7. Panel (a): low temperature $g_2(r)$ for the three axes ($g_{2aa}(r), g_{2bb}(r)$ and g_{2cc}, green, orange and black lines, respectively). Panel (b) high temperature $g_{2aa}(r), g_{2bb}(r)$ and g_{2cc} (green, orange and black lines, respectively). A first pronounced peak is appreciable for the system at high temperature.

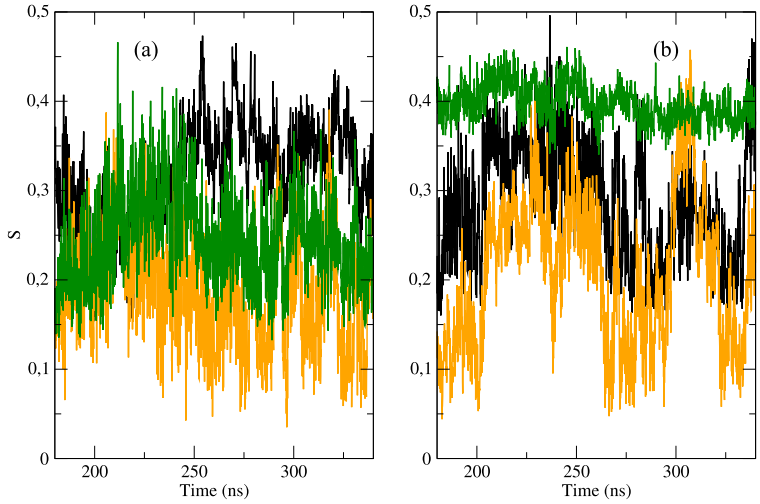

Fig. 8. Nematic order parameter S_{aa}, S_{bb} and S_{cc} for low temperature (panel (a)) and for high temperature (panel (b)) as a function of the time (green, orange and black lines, respectively).

In colloidal physics, solutions made of polydisperse anisotropic elongated (rod like, ellipsoidal) hard particles are known to present a liquid crystalline (LC) phase if the ratio $A = L/D$ between the average elongation L of the particle and its diameter D overcomes a minimum threshold $A_{\min} \in (3, 4]$ [44,45]. For these systems, a polydispersity in length was shown not to alter the phase diagram with respect to the one obtained for the corresponding monodisperse system, while a polydispersity in diameter might affect the concentration at which a LC phase is observed [46,47], without nevertheless suppressing it. The just described coarse grained methodology, allows us to map the atomistic macromolecules onto anisotropic hard ellipsoids "colloidal like" particles, whose aspect ratio allows us to hypothesise that the macromolecules should be LC former. This assumption is strengthened by the results obtained at finite concentration in our simulations, that show a pre-nematic order for the high temperature cases. We can thus infer that high temperature PiPOx solutions, for DPs that are sufficiently short not to be too flexible to have a LC order, but long enough to have the minimal aspect ratio required for the Isotropic/Nematic transition, should present - for a range of concentrations - a liquid crystalline phase.

Finally, its is proposed in literature that weak hydrogen bonds (weak HBs) may form between the methyl groups in the isopropyl side chains, and the carbonyl oxygens. In fact, such weak hydrogen bonds were observed experimentally by means of IR measurements within aqueous solutions of PiPOx and it is suggested that the breakage of these interactions may be the starting point of the conformational rearrangement eventually leading to the stretched conformations that characterise the de-mixing condition [10]. We addressed this point by analysing the number of both inter and intra molecular $CH_3 \cdots O{=}C$ weak HBs within the $T = T_L$ and $T = T_H$ simulations. However, while the observation that such interactions take place within these systems is supported by our simulations, they do not seem to dramatically affect neither the stable solution nor the de-mixing condition (see SI, Section 3.1 for the complete analyses). However, a slight increase in the number of intermolecular hydrogen bonds is observed at high temperature, suggesting that this interaction may play a role in driving or stabilising condensation.

3.3. *The contribution from hydration*

In the previous section we have extensively discussed that, above the de-mixing temperature, the water-PiPOx system is dominated by the inter-chain interactions that lead to LLPS, with polymers adopting regular elongated conformations, that we have demonstrated to be reminiscent of the ones adopted by the macromolecules in the crystalline phases. Still, the role of hydration in this change in conformation remains to be addressed. In fact, the differential features characterising

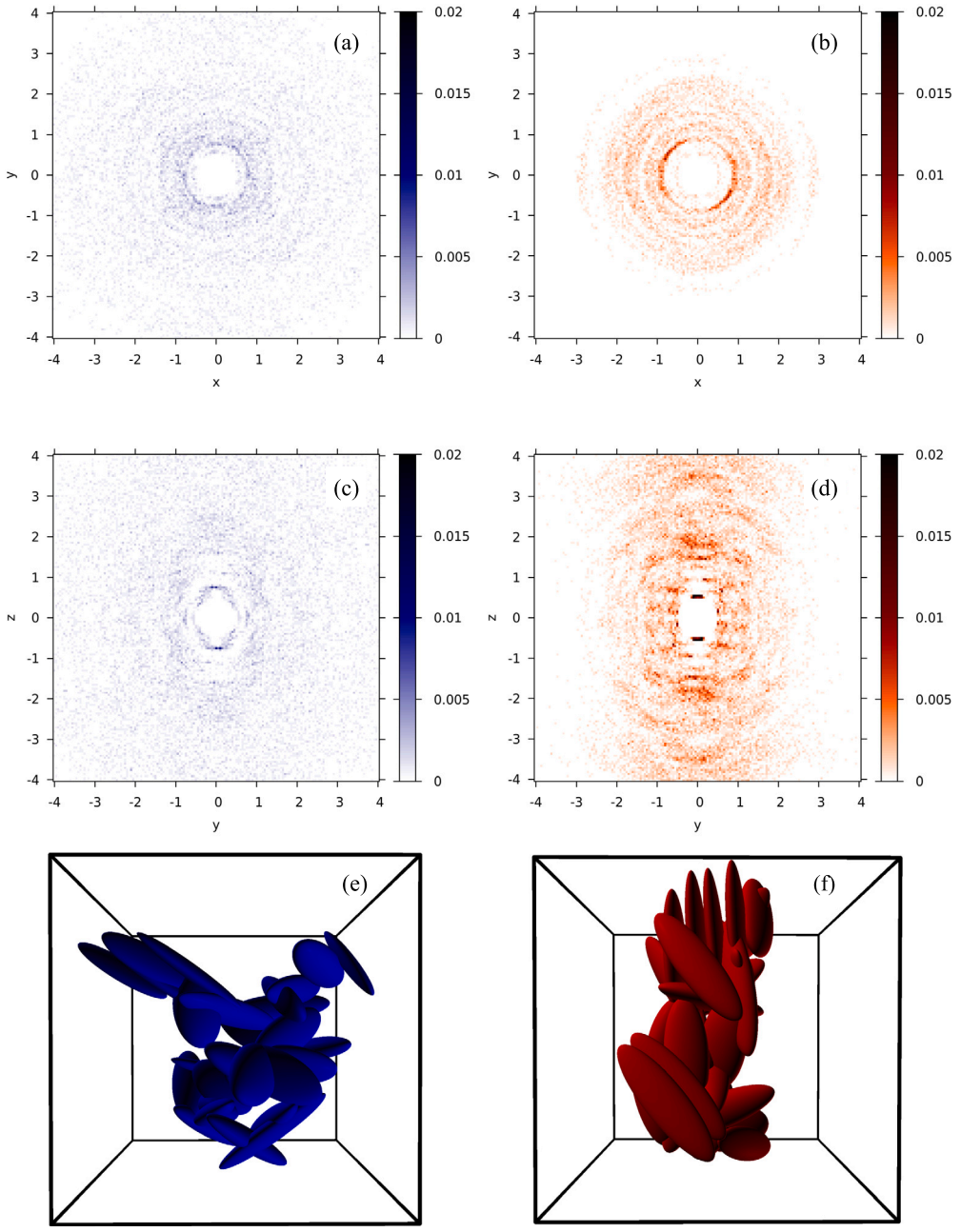

Fig. 9. Projection of the three dimensional $g(r)$ on the $z = 0$ and $x = 0$ planes for low temperature (panel (a) and (c) respectively) and for high temperature (panel (b) and (d) respectively). Representative snapshots from the T_L (panel (e)) and T_H (panel (f)) simulations showing the polymer chains according to the ellipsoid-based coarse grained representation. The T_L ellipsoids are represented in blue, the T_H ones, in red.

the systems at the different temperatures may concur to the preferential polymer-polymer interactions dominating in the polymer rich phase after de-mixing.

In order to address this point, we started by analysing the hydration of the single chains by computing the ρ/ρ_{fict} profile (see Methods) for the PiPOx10, PiPOx20 and PiPOx30 molecules at infinite dilution, for the two temperatures, as reported in Fig. 10, panels (a), (b), (c) (the results obtained from the replicas are reported in the SI, Section 4.1). From the analysis of the water density profile, we can deduct the influence that the presence of a polymer exerts on the water density around the macromolecule, as a function of the distance from the polymer. The plateau $\rho/\rho_{\text{fict}} = 1$ - indicating that the density of water around the molecule coincides with water density in the bulk - is reached for a distance of about $r_{\text{hyd}} \in [0.7, 1]$ nm from the polymer surface. The features of ρ/ρ_{fict} in the region $r < r_{\text{hyd}}$ define the properties of the hydration shell: with reference to Fig. 10 it clearly appears that no striking differences can be appreciated within the hydration shells for the two T_L and T_H temperatures analysed. To quantify, by considering $r_{\text{hyd}} = 1$ nm we obtain an increase in water density of about 6% for both the T= 283 K and T= 323 K systems due to the presence of the polymer with respect to the bulk (see Methods for the procedure; given that no size-dependent trend is observed, the water density increase is obtained by averaging the data from the three different solutes for each temperature). While no relevant density changes are observed between the systems for the two temperatures, a temperature related effect can be quantified by an analysis of the average number of molecules surrounding the polymer. As a matter of fact, the hydration effects can be highlighted by computing the number of water molecules enclosed within the ellipsoid that best approximates each polymeric surface, that can be considered as a good approximation of the first hydration layer (N_{wat}).

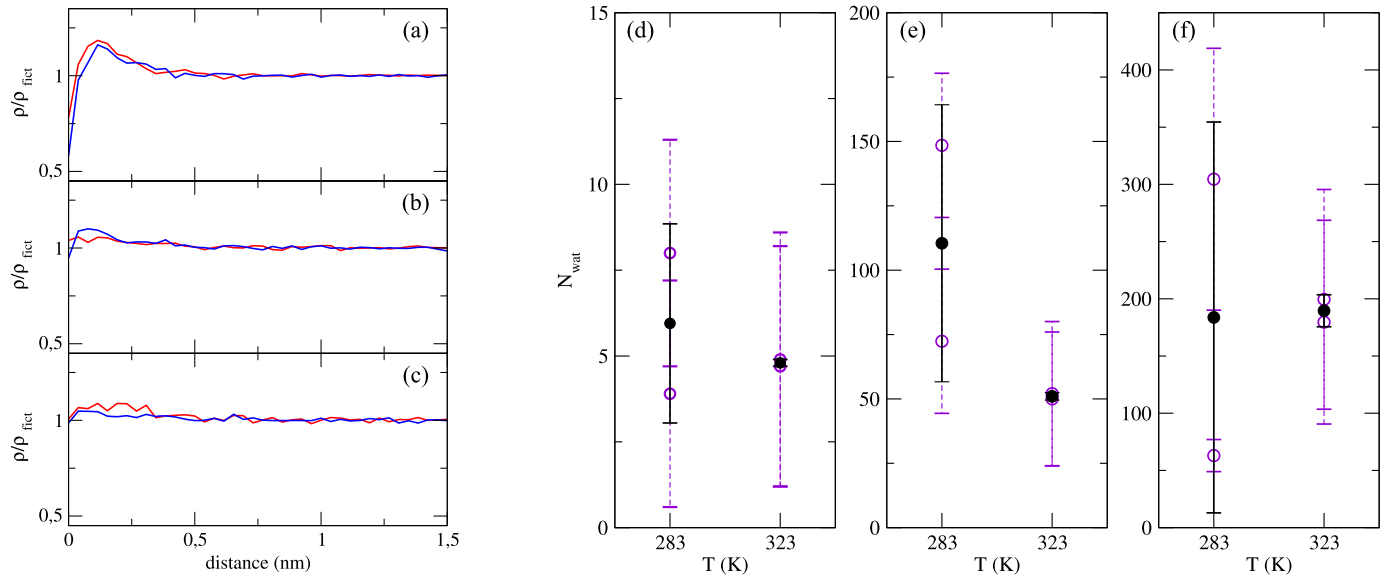

Fig. 10. Comparison between the water density ρ computed in the presence of the polymer, and the water density in bulk condition ρ_{fict} (see Methods) for increasing distances from the ellipsoidal surface that approximates PiPOx10 (panel (a)), PiPOx20 (panel (b)) and PiPOx30 (panel (c)) at T= 283K (blue line) and T= 323 K (red line). Number of water molecules closest to the polymeric chains (namely those enclosed within the polymer ellipsoidal surface) for two different replicas at T= 283 K and T= 323 K (purple points and dashed errorbars), and the average computed over the two replicas for the two temperatures in black for PiPOx10 (panel (d)), PiPOx20 (panel (e)) and PiPOx30 (panel (f)). The errors computed on each replica are a measure of the fluctuation within every single simulations, and the standard deviations on the two replicas are a measure of the variability of two independent measurements. While the comparison of the density profiles for the two analysed temperature presents similar features for the analysed molecules, with an increase in water density close to the solute surface, the number of water molecules involved in the density increment instead is greater for the low temperature case ($N_{\text{wat,T=283}}/N_{\text{wat,T=323}} > 1$ for PiPOx10 and PiPOx20, and $N_{\text{wat,T=283}}/N_{\text{wat,T=323}} \sim 1$ for PiPOx30.)

As reported in panels (d), (e), (f) of Fig. 10, irrespective of the solute analysed, the number $N_{\text{wat,T=323}}$ of water molecules hydrating the polymer at short distances and high temperature is lower than the $N_{\text{wat,T=283}}$ value obtained computing the water molecules hydrating the macromolecules at the lowest temperature analysed, on average. The average was computed over the two performed replicas. We report both data averaged over every single trajectory (replica), as well as the average obtained over the two independent replicas. Low temperature presents a wider fluctuation, while higher temperature presents less fluctuation within every single simulation. The average value obtained is reported with an error corresponding to the standard deviation between the two different replicas, while the errors reported for each replica are a measure of the intra-simulation fluctuations. It is hence found that $N_{\text{wat,T=283}}/N_{\text{wat,T=323}} > 1$ for PiPOx10 and PiPOx20, and $N_{\text{wat,T=283}}/N_{\text{wat,T=323}} \sim 1$ for PiPOx30.

It follows that the partially folded conformations adopted by the polymer at low temperature are stabilised by a greater number of hydration water molecules with respect to the stretched conformations characterising the high temperature. Hence, it might be arguable that the decrease in the entropic cost related to the number of degrees of freedom of water quenched by hydration observed at high temperature concurs in the acquisition of the stretched unfolded conformations at high T.

Finally, we repeat the just described procedure to analyse the finite dilute simulations. The ρ/ρ_{fict} profiles for the two T_H and T_L temperatures and $x_w = 0.1$ are reported in panel (a) of Fig. 11 (the results obtained from the replica are reported in the SI, Section 4.2). As mentioned for the infinite dilution case, the plateau value reflects the density of water at large distance from the polymer chain, hence being a measure of the average water density in solution. On the contrary, the values corresponding to small distances define the properties of the polymer hydration shell. While all hydration curves appeared to be very similar for the two analysed temperatures at infinite dilution for all solutes, moving to a finite concentration induces an appreciable temperature related effect on the single molecule hydration. As a matter of fact, the ρ/ρ_{fict} curves obtained for the T_L and T_H simulations appear to be quite different, as shown in panel (a) of Fig. 11.

The profile obtained for T= 283 K presents two main features: i) at least two peaks of increased density are observed around the polymer chains, ii) the water density plateau is higher than 1. The former aspect confirms that, even if the polymeric chains at low temperature are interacting (see previous Results 3.2 section), they are well hydrated and do not form aggregates that modify the single chain level hydration features. Instead, moving to $r > r_{\text{hyd}}$ the value $\rho/\rho_{\text{fict}} > 1$ indicates that, on average, water is at a density higher than that of bulk. This is due the presence of a multitude of solutes, each one well hydrated - as demonstrated by the peaks at short distance in the plots. The high content of hydration water, thus, collectively affects the average water density which results to be slightly higher than the bulk (this phenomenon is better analysed in ref. [34]).

Interestingly, in the T= 323 K case, the ρ/ρ_{fict} profile does not resemble the one of a typical solute in water; close to the chain surface, the density is smaller than that of bulk and the plateau is hardly reached. These aspects are due to the formation of the large aggregate described in the previous section. In fact, within such a supramolecular structure, only the regions of the polymer chains at the interface can be genuinely considered to be hydrated. The ratio smaller than 1 between the density computed from the actual simulation and the “fictitious” one, are due to regions of low density within the actual simulation that would contain more water molecules in the “fictitious” condition. By increasing the distance from the polymer surface, the density of water is affected according to three regimes: the $r << r_{\text{hyd}}$ low density regions, the hydration layers surrounding the large cluster ($r \simeq r_{\text{hyd}}$), and the $r >> r_{\text{hyd}}$ regions (distant from the cluster surface) where water can be assumed to be in bulk condition. This gives rise to the peculiar shape of the ρ/ρ_{fict} curve of Fig. 11 panel (a) for T= 323 K.

Finally, we computed the number of hydrogen bonds (HB) between water and the polymer, as we report in panel (b) of Fig. 11 (the results obtained from the replica are reported in the SI, Section 4.3). The data are reported normalised by the maximum number of HBs between

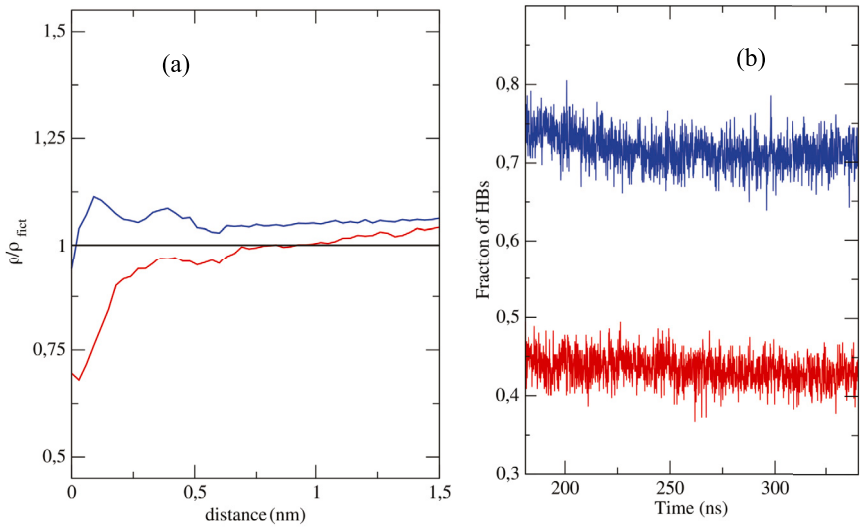

Fig. 11. Panel (a): Comparison between the water density ρ computed in presence of the polymer, and the water density in bulk condition ρ_{fict} for increasing distances from the ellipsoidal surface that approximates PiPOx10 at $x_w = 0.1$ and T= 283 K (blue line) and T= 323 K (red line). For clarity, a black line corresponding to $\rho/\rho_{\text{fict}} = 1$ is reported. Panel (b): Fraction of hydrogen bonds (HB) engaged by the polymer with water (the reference for the normalisation is given by the number of HB between Pipox10 and water obtained from the single chain simulations at the two temperatures).

the solute and the solvent. The latter is obtained - for each temperature - as the number of HBs between PiPOx10 and water computed from the single molecule simulation, multiplied by the number of chains in solution. While at low temperature, almost all the possible HBs are satisfied (fraction of HBs greater than 0.7), at high temperature less than half of the maximum number of bonds are made. This confirms that large part of the big cluster that is found at high temperature remains not hydrated. Moreover, in literature it is also proposed that peculiar hydrogen bonds are formed between PiPOx and water, bridging two carbonyl groups [48]. Such cross-linking bonds are predicted to induce liquid-liquid phase separation as a step prior to water expulsion and formation of the polymer-rich phase [10]. From the MD simulations, we observe that few of these bonds form. On average, we compute ~ 0.3 bonds per frame, per chain, for both systems; this means that around 30% of the total acceptors are involved in the bridging for each system. Hence, according to our data, such a property does not seem to actually characterise neither the stable solution nor the de-mixing condition. However, when $T = T_H$, the few bridges that are found, are located at the interface between the polymer rich and the water rich phases (see SI, Fig. S15, for a snapshot of the system). To conclude, in line with the single molecule analyses, these results stress the major role played by hydration in the thermoresponsive behaviour of PiPOxs. In particular, our data confirm the resemblance between LCST and the liquid-liquid phase separation reported in literature.

4. Conclusions

This work represents the first extensive molecular dynamics investigation of poly(2-isopropyl-2-oxazoline) addressing the nature of the thermoresponsive behaviour of this polymer both at infinite dilution and finite concentration. To this aim, three different systems (DP = 10, 20, 30) - with two replicas each - have been simulated at infinite dilution for three different temperatures, $T_L = 283$ K that we expect to be well below the experimental LCST, $T_R = 300$ K and $T_H = 323$ K, T_R expected to be about LCST, and T_H to be above. We then explored the temperature influence on structural properties of finite concentration solutions for the DP = 10 system at T_L and T_H, with two independent replicas containing a different number of polymer chains for a fixed concentration, to have a control over possible size effects.

The thermoresponsiveness lies in a change of solubility for PiPOx aqueous solutions, that undergo a transition from a state with well-solvated polymer chains (thus appearing limpid at sight) up to a liquid-liquid phase separation - LLPS - where solutions become turbid. Moreover, poly(2-isopropyl-2-oxazoline) in water is experimentally known to crystallise at temperatures well above LCST, or around LCST if left unperturbed for a long time.

While crystals are easy to characterise by means of X-ray diffraction (XRD) methods, accessing structural information for de-mixed phases is more difficult. Moreover, to date, an extensive study that would provide an explanation at the molecular level of the nature of the thermoresponsiveness of the polymer, is lacking.

To start the exploration, we first of all assess the validity of our newly developed PiPOx model, by comparing diffusion coefficient results from simulations with those obtained by DLS measurements on specifically synthesised polymers of controlled DP. We use such a favourable comparison to confirm the predictability of our model over experimental findings.

Single chain simulations performed at different temperatures show a difference in the average polymer conformation, that results to be significantly more stretched at higher temperature. While chain at low temperature tends to assume bent conformations, at high temperature the configurational space of possible conformations is restricted to very stretched macromolecular conformations. This feature is reproduced for all analysed DPs, and well matches with the structural characteristics experimentally detected (by IR, NMR methods) for the polymer rich phase in de-mixing condition.

Given such an effect, it is interesting to analyse the role played by water in the two different states, at the different temperatures. We find that high temperature systems are characterised by smaller hydration shells, and hypothesise that the shrinking of the hydration shell upon increasing temperature concurs to the high temperature stretching of this water soluble polymer.

The thermoresponsive behaviour is even more pronounced at finite concentration of PiPOx, where the temperature increase triggers an intermolecular aggregation process, that leads to the expulsion of water molecules from the polymer rich phase, thus inducing a micro phase separation (LLPS).

To better explore the nature of the polymer rich phase, we performed a coarse graining by remapping every atomistically defined polymer chain onto an effective ellipsoid, and by then measuring the average angular and radial distribution of such ellipsoids. We found that structures self-assembled at high temperature, present a local liq-

uid crystalline (LC) ordering. We can thus hypothesise that polymers with DPs sufficiently long for the macromolecule to have the needed anisotropy, and short enough to remain reasonably rigid, at high temperature should form a liquid crystalline phase in the LLPS region. Such a property would allow to have fully controllable thermoresponsive liquid crystals, thus electing PiPOx systems as optimal candidates for optical thermoresponsive switchers. The existence of the LC phase, as well as the exploration of the possible thermodynamic conditions that would lead to a stable LC phase, are currently being analysed in our laboratory, and will be the subject of future contributions.

CRediT authorship contribution statement

All authors contributed equally to the work.

Declaration of competing interest

The authors declare that they have no known competing financial interests or personal relationships that could have appeared to influence the work reported in this paper.

Data availability

Data will be made available on request.

Acknowledgements

SDG would like to acknowledge the funding “Ricerca e Innovazione” 2014-2020 D.M. 1423. 16-09-2022. SDG, CADF, LS, TG and BC would like to acknowledge the Grant of Excellence Departments, MIUR-Italy (ARTICOLO 1, COMMI 314 - 337 LEGGE 232/2016). All authors acknowledge CINECA for providing computing time on HPC facilities.

Appendix A. Supplementary material

Supplementary material related to this article can be found online at https://doi.org/10.1016/j.molliq.2023.123420.

References

[1] R. Hoogenboom, H. Schlaad, Thermoresponsive poly(2-oxazoline)s, polypeptoids, and polypeptides, Polym. Chem. 8 (2017) 24–40, https://doi.org/10.1039/C6PY01320A.
[2] M. Glassner, M. Vergaelen, R. Hoogenboom, Poly(2-oxazoline)s: a comprehensive overview of polymer structures and their physical properties, Polym. Int. 67 (2018) 32–45, https://doi.org/10.1002/pi.5457.
[3] S. Huber, N. Hutter, R. Jordan, Effect of end group polarity upon the lower critical solution temperature of poly(2-isopropyl-2-oxazoline), Colloid Polym. Sci. 286 (2008) 1653–1661.
[4] V. Ďordovič, B. Verbraeken, R. Hogenboom, S. Kereïche, P. Matějíček, M. Uchman, Tuning of thermoresponsivity of a poly(2-alkyl-2-oxazoline) block copolymer by interaction with surface-active and chaotropic metallacarborane anion, Chem. - Asian J. 13 (2018) 838–845, https://doi.org/10.1002/asia.201701720.
[5] S. Jana, M. Uchman, Poly(2-oxazoline)-based stimulus-responsive (Co)polymers: an overview of their design, solution properties, surface-chemistries and applications, Prog. Polym. Sci. 106 (2020) 101252, https://doi.org/10.1016/j.progpolymsci.2020.101252.
[6] E. Roma, P. Corsi, M. Willinger, N.S. Leitner, R. Zirbs, E. Reimhult, B. Capone, T. Gasperi, Theoretical and experimental design of heavy metal-mopping magnetic nanoparticles, ACS Appl. Mater. Interfaces 13 (2021) 1386–1397, https://doi.org/10.1021/acsami.0c17759, PMID 33389993.
[7] E. Roma, P. Corsi, B. Capone, E. Reimhult, T. Gasperi, Thermoresponsive block copolymer grafted on core-shell nanoparticles, AIP Conf. Proc. 2416 (2021) 020018, https://doi.org/10.1063/5.0069698.
[8] J. Zhao, R. Hoogenboom, G. Van Assche, B. Van Mele, Demixing and remixing kinetics of poly(2-isopropyl-2-oxazoline) (PIPOZ) aqueous solutions studied by modulated temperature differential scanning calorimetry, Macromolecules 43 (2010) 6853–6860, https://doi.org/10.1021/ma1012368.
[9] Y. Katsumoto, A. Tsuchiizu, X. Qiu, F.M. Winnik, Dissecting the mechanism of the heat-induced phase separation and crystallization of poly(2-isopropyl-2-oxazoline) in water through vibrational spectroscopy and molecular orbital calculations, Macromolecules 45 (2012) 3531–3541.
[10] T. Li, H. Tang, P. Wu, Molecular evolution of poly(2-isopropyl-2-oxazoline) aqueous solution during the liquid–liquid phase separation and phase transition process, Langmuir 31 (2015) 6870–6878.
[11] S. Sun, P. Wu, Conformational changes in the heat-induced crystallization of poly(2-isopropyl-2-oxazoline) in the solid state, Phys. Chem. Chem. Phys. 17 (2015) 31084–31092, https://doi.org/10.1039/C5CP05719A.
[12] C. Diehl, P. Černoch, I. Zenke, H. Runge, R. Pitschke, J. Hartmann, B. Tiersch, H. Schlaad, Mechanistic study of the phase separation/crystallization process of poly(2-isopropyl-2-oxazoline) in hot water, Soft Matter 6 (2010) 3784–3788, https://doi.org/10.1039/C0SM00114G.
[13] M. Meyer, M. Antonietti, H. Schlaad, Unexpected thermal characteristics of aqueous solutions of poly(2-isopropyl-2-oxazoline), Soft Matter 3 (2007) 430–431, https://doi.org/10.1039/B616678D.
[14] A.L. Demirel, M. Meyer, H. Schlaad, Formation of polyamide nanofibers by directional crystallization in aqueous solution, Angew. Chem., Int. Ed. 46 (2007) 8622–8624, https://doi.org/10.1002/anie.200703486.
[15] T. Furuncuoğlu Özaltın, V. Aviyente, C. Atılgan, L. Demirel, Multiscale modeling of poly(2-isopropyl-2-oxazoline) chains in aqueous solution, Eur. Polym. J. 88 (2017) 594–604, https://doi.org/10.1016/j.eurpolymj.2016.10.013.
[16] M. Abraham, T. Murtola, R. Schulz, S. Páll, J. Smith, B. Hess, E.G.RO.MA. CS Lindahl, High performance molecular simulations through multi-level parallelism from laptops to supercomputers, SoftwareX, https://doi.org/10.5281/zenodo.4054996.
[17] J.L.F. Abascal, E. Sanz, R. García Fernández, C. Vega, A potential model for the study of ices and amorphous water: TIP4P/Ice, J. Chem. Phys. 122 (2005) 234511, https://doi.org/10.1063/1.1931662.
[18] W.L. Jorgensen, D.S. Maxwell, J. Tirado-Rives, Development and testing of the OPLS all-atom force field on conformational energetics and properties of organic liquids, J. Am. Chem. Soc. 118 (1996) 11225–11236, https://doi.org/10.1021/ja9621760.
[19] B. Chandramouli, S. Del Galdo, G. Mancini, N. Tasinato, V. Barone, Tailor-made computational protocols for precise characterization of small biological building blocks using QM and MM approaches, Biopolymers 109 (2018) e23109, https://doi.org/10.1002/bip.23109.
[20] L.S. Dodda, I. Cabeza de Vaca, J. Tirado-Rives, W.L. Jorgensen, LigParGen web server: an automatic OPLS-AA parameter generator for organic ligands, Nucleic Acids Res. (2017) W331–W336.
[21] A.D. Becke, Density-functional exchange-energy approximation with correct asymptotic behavior, Phys. Rev. A 38 (1988) 3098–3100.
[22] M.J. Frisch, et al., Gaussian09 Revision E.01, Gaussian Inc., Wallingford CT, 2009.
[23] D. Case, et al., Amber 2022, University of California, San Francisco, 2022.
[24] L. Tavagnacco, E. Chiessi, E. Zaccarelli, Molecular insights on poly(N-isopropylacrylamide) coil-to-globule transition induced by pressure, Phys. Chem. Chem. Phys. 23 (2021) 5984–5991, https://doi.org/10.1039/D0CP06452A.
[25] H.J.C. Berendsen, J.P.M. Postma, W.F. van Gunsteren, A. Di Nola, J.R. Haak, Molecular dynamics with coupling to an external bath, J. Chem. Phys. 81 (1984) 3684–3690, https://doi.org/10.1063/1.448118.
[26] G. Bussi, D. Donadio, M. Parrinello, Canonical sampling through velocity rescaling, J. Chem. Phys. (2007) 126.
[27] B. Hess, H. Bekker, H.J.C. Berendsen, J.G.E.M. Fraaije, LINCS: a linear constraint solver for molecular simulations, J. Comput. Chem. 18 (1997) 1463–1472.
[28] T. Darden, D. Tork, L. Pedersen, Particle mesh Ewald: an N-log(N) method for Ewald sums in large systems, J. Comput. Chem. 18 (1997) 1463–1472.
[29] S. Del Galdo, P. Marracino, M. D’Abramo, A. Amadei, In silico characterization of protein partial molecular volumes and hydration shells, Phys. Chem. Chem. Phys. 17 (2015) 31270–31277, https://doi.org/10.1039/C5CP05891K.
[30] S. Del Galdo, A. Amadei, The unfolding effects on the protein hydration shell and partial molar volume: a computational study, Phys. Chem. Chem. Phys. 18 (2016) 28175–28182, https://doi.org/10.1039/C6CP05029H.
[31] A. Amadei, S.D. Galdo, M. D’Abramo, Density discriminates between thermophilic and mesophilic proteins, J. Biomol. Struct. Dyn. 36 (2018) 3265–3273.
[32] L. Zanetti-Polzi, A.D. Biswas, S. Del Galdo, V. Barone, I. Daidone, Hydration shell of antifreeze proteins: unveiling the role of non-ice-binding surfaces, J. Phys. Chem. B 123 (2019) 6474–6480, https://doi.org/10.1021/acs.jpcb.9b06375, PMID: 31280567.
[33] A.D. Biswas, V. Barone, A. Amadei, I. Daidone, Length-scale dependence of protein hydration-shell density, Phys. Chem. Chem. Phys. 22 (2020) 7340–7347, https://doi.org/10.1039/C9CP06214A.
[34] S. Del Galdo, M. Chiarini, C. Casieri, I. Daidone, High density water clusters observed at high concentrations of the macromolecular crowder PEG400, J. Mol. Liq. 357 (2022) 119038.
[35] B.D. Monnery, S. Shaunak, M. Thanou, J.H. Steinke, Improved synthesis of linear poly (ethylenimine) via low-temperature polymerisation of 2-isopropyl-2-oxazoline in chlorobenzene, Macromolecules 48 (2015) 3197–3206.
[36] K. Kempe, M. Lobert, R. Hoogenboom, U.S. Schubert, Screening the synthesis of 2-substituted-2-oxazolines, J. Comb. Chem. 11 (2009) 274–280.
[37] B. Verbraeken, B.D. Monnery, K. Lava, R. Hoogenboom, The chemistry of poly (2-oxazoline)s, Eur. Polym. J. 88 (2017) 451–469.
[38] H.S. Dhadwal, R.R. Ansari, W.V. Meyer, A fiber-optic probe for particle sizing in concentrated suspensions, Rev. Sci. Instrum. 62 (1991) 2963–2968.
[39] C.L. Lawson, R.J. Hanson, Solving Least Squares Problems, SIAM, 1995.
[40] M.P. Allen, D.J. Tildesley, Computer Simulation of Liquids, Clarendon Press, Oxford, 1987.

[41] P.G. de Gennes, T.A. Witten, Scaling concepts in polymer physics, Phys. Today 33 (1980) 51–54, https://doi.org/10.1063/1.2914118.
[42] M. Litt, F. Rahl, L.G. Roldan, Polymerization of cyclic imino ethers. VI. X-ray study of some polyaziridines, J. Polym. Sci., Part A-2, Polym. Phys. 7 (1969) 463–473, https://doi.org/10.1002/pol.1969.160070302.
[43] F. Eisenhaber, P. Lijnzaad, P. Argos, C. Sander, M. Scharf, The double cubic lattice method: efficient approaches to numerical integration of surface area and volume and to dot surface contouring of molecular assemblies, J. Comput. Chem. 16 (1995) 273–284, https://doi.org/10.1002/jcc.540160303.
[44] S.C. McGrother, D.C. Williamson, G. Jackson, A re-examination of the phase diagram of hard spherocylinders, J. Chem. Phys. 104 (1996) 6755–6771, https://doi.org/10.1063/1.471343.
[45] A. Pal, C.A. De Filippo, T. Ito, M.A. Kamal, A.V. Petukhov, C. De Michele, P. Schurtenberger, Shape matters in magnetic-field-assisted assembly of prolate colloids, ACS Nano 16 (2022) 2558–2568, https://doi.org/10.1021/acsnano.1c09208.
[46] M. Bates, D. Frenkel, Influence of polydispersity on the phase behavior of colloidal liquid crystals: a Monte Carlo simulation study, J. Chem. Phys. (1998) 109, https://doi.org/10.1063/1.477248.
[47] C.A. De Filippo, S. Del Galdo, P. Corsi, C. De Michele, B. Capone, On the role of polydispersity on the phase diagram of colloidal rods, Soft Matter 19 (2023) 1732–1738, https://doi.org/10.1039/D2SM01355J.
[48] C. Calero, G. Franzese, Membranes with different hydration levels: the interface between bound and unbound hydration water, J. Mol. Liq. 273 (2019) 488–496, https://doi.org/10.1016/j.molliq.2018.10.074.